Habilitation thesis

Light reflection from structured media

by

Dr. Alexander Petrov

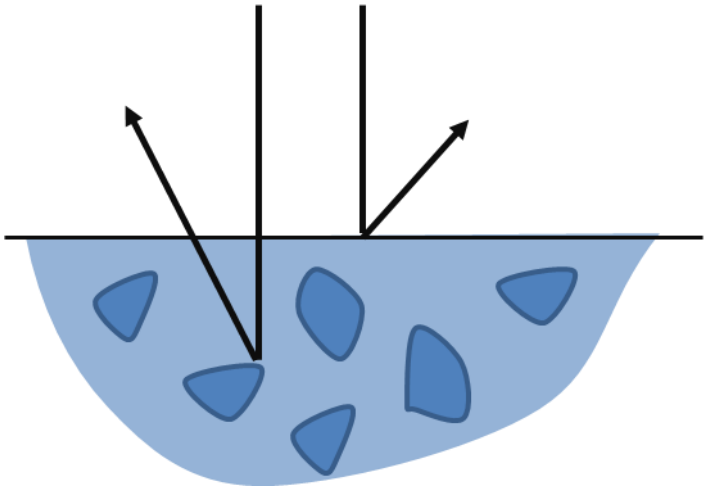

Hamburg University of Technology

Institute of Optical and Electronic Materials

Hamburg, 2023

Habilitation submitted: 11.11.2021

Habilitation colloquium: 21.04.2022

Acknowledgement

This habilitation thesis is based on several publications from 2012 till 2018 written in the Institute of Optical and Electronic Materials (OEM) at TUHH. The completion of this work would not have been possible without the valuable contributions and support from numerous individuals, whom I would like to acknowledge here.

First of all, I extend my gratitude to the master's, PhD and PostDoc students of OEM institute who played pivotal roles in this endeavor as first authors of the presented publications: Simone Fohrmann, Clark (Hooi Sing) Lee, Pavel Dyachenko, Lukas Maiwald, Guoliang Shang, Slawa Lang, Dirk Jalas, Michel Castellanos Muñoz, Elena Ulchenko, Mahmoud Gaafar. Their direct contributions have been instrumental in realizing many of the concepts and ideas presented within these papers. Especially I would like to thank Dirk, with whom I discussed and developed many of the ideas presented here. My thanks also extend to other students, researchers, technicians, and the institute's administrative staff for their consistent support.

I am deeply indebted to Prof. Manfred Eich, who not only provided me with the platform to develop my ideas within his institute but also offered invaluable guidance and assistance and encouraged me to pursue the submission of this habilitation thesis. His unwavering belief in my capabilities is sincerely appreciated.

The realization of a significant portion of the publications featured in this thesis was made possible through financial support from the German Research Foundation (DFG), particularly via the Collaborative Research Center 986 (SFB 986) focused on multiscale materials. The work in SFB 986 significantly influenced my interest in the interaction of light with structured media. I extend my thanks to DFG and all collaborators involved in the SFB 986 projects for their contributions to my research journey.

My wife, Maria, has been my pillar of support throughout these years. I am immensely grateful for her encouragement and understanding. I also wish to express my gratitude to my parents for their continual support.

Contents

1. Summary

The possibilities for material structuring and composition on nano and micrometer level have allowed new optical functionalities unavailable with bulk materials. For example, the combination of metals and dielectrics as alternating nanolayers provides a novel anisotropic medium with wave numbers approaching infinity in some directions, so called hyperbolic media. The properties of structured media are strongly dependent on geometry. If structural elements are much smaller than the wavelength of light in constituting materials, then the optical properties of the structured media can be described by effective medium parameters. In this case the structured medium represents a metamaterial. If structural elements are comparable to the wavelength, then the phase of light and interference effects should be considered. In the case of periodical structures, so-called photonic crystals, again effective propagation parameters can be defined for the so-called Bloch modes which propagate unperturbed through the periodic structure. Structures without periodicity are more difficult to describe, and approximate theories are applied to determine scattering. The structural elements much larger than the wavelength are in the realm of geometrical optics and are not considered here.

In this cumulative habilitation thesis, I discuss a particular effect of interaction with structured media, namely the reflection of light. In conventional media the reflection is observed at the boundary between two media, and it is described by the Fresnel equations. For metamaterials, the Fresnel equations can be also applied. In this case the reflection can be changed by the adjustment of the structure and thus the effective medium parameters. For photonic crystals and disordered media, the situation becomes more complex and Fresnel equations are not applicable anymore. Exact consideration of the boundary between structured medium and the input material should be considered. Reflection can build up via accumulation of scattering in the volume of the second medium or due to absence of propagating modes. A special case of reflection is considered when boundary between two media is moving, which leads not only to the change of direction of light but also the frequency. For each of the presented media special theoretical approaches were developed and applied to optimize the reflection properties for envisaged applications.

This habilitation work is based on 14 publications published in the last 10 years. They are chosen based on novelty, most of these publications resulted in several follow up publications which are also briefly mentioned in this thesis. Following reflection effects are considered:

- Broadband omnidirectional reflection (3 publications),
- Spectrally selective omnidirectional reflection (3 publications),
- Suppressed reflection for selective absorption (3 publications)
- Broadband absorption (2 publications)
- Reflection from a moving front (3 publications)

Omnidirectional broadband reflection is important for several applications. We have utilized it to keep light for a long time in a small area on a chip and to protect surfaces from thermal radiation. For that chirped and multistack photonic crystals were developed, as well as disordered structures. It was possible to realize efficient reflectors with better than 99% reflectivity to keep light in confined area on a silicon chip. Also, thermally stable disordered reflectors with 80% reflectivity of thermal radiation from 1 to 6 μm range were demonstrated for the application as thermal barrier coatings. Spectrally selective reflectors

were developed for structural color application with blue color saturation approaching that of monochromatic light. To avoid angle dependence disordered structures were used based on a densely packed arrangement of spheres, so-called photonic glass. For thermophotovoltaics, conversion of thermal radiation into electric power, selective thermal emitters were developed with spectral efficiency approaching 50% and temperature stability at 1400 °C. The spectral selectivity was based on metal-dielectric multilayer metamaterials and metal-dielectric photonic crystals allowing reflection of long wavelength photons and absorption/emission of short wavelength photons. Also, broadband absorbers for visible light based on nanoporous gold metamaterial were theoretically described. Reflectivity of nonporous gold was tuned by applied electric voltage. Finally, the Doppler-like reflection from moving refractive index front was described and realized experimentally, which can be applied for frequency and bandwidth manipulation of optical signals.

2. Background

Here I introduce several concepts that were applied in the publications. A detailed review of the state of art is presented in each of the presented publications and will not be repeated here.

In this work structured media are considered consisting of at least two media. In general, structured media can be described by position dependent relative permittivity $\varepsilon(\vec{r})$. In this thesis we neglect the magnetic response of the materials at optical frequencies: $\mu(\vec{r}) = 1$. The structures media from two materials can be split in the volumes with relative permittivity ε_1 and ε_2, where one of the materials can be vacuum with relative permittivity equal to 1.

The permittivity of the constituent materials can be approximately constant in the considered wavelength range but is generally a function frequency. As dielectric materials are considered away from absorption resonances here, we assume a constant permittivity with negligible loss. It should be mentioned that semiconductors like silicon are generally considered as dielectric materials in optics with approximately constant dielectric permittivity. But for the metals the frequency dependence of permittivity must be taken into account due to the broadband contribution of free electrons. A free electron with charge e and mass m moving in the oscillating electric field E and damped with rate γ is described by second order differential equation:

$$m(\ddot{x} + \gamma\dot{x}) = -eE \tag{1}$$

where electron position $x(t)$ is changing with time. Taking a Fourier transform of this equation a frequency dependent oscillation amplitude is obtained:

$$m(-\omega^2 - i\gamma\omega)\hat{x} = -e\hat{E} \tag{2}$$

$$\hat{x}(\omega) = \frac{e\hat{E}}{m(\omega^2 + i\gamma\omega)} \tag{3}$$

Thus, displacement of electrons is proportional to applied electric field. As there is no restoring force, there is no resonant increase of oscillation amplitude at a certain frequency. At large frequency the displacement strongly decreases.

As the polarization of the medium is connected to the dipole moment of electrons $-e\hat{x}$ and their concentration n_e, the electric susceptibility χ_e and finally the permittivity can be written as:

$$\varepsilon = \varepsilon_b + \chi = \varepsilon_b - \frac{\omega_p^2}{\omega^2 + i\gamma\omega} \tag{4}$$

where ε_b is the background permittivity due to bound electrons and plasma frequency ω_p is equal to $\sqrt{\frac{n_e e^2}{m\varepsilon_0}}$ with ε_0 being the permittivity of vacuum.

The damping rate γ is also called collision frequency of electrons. In this case the collisions that can damp the collective motion of electrons are considered, such as collisions with lattice defects, phonons and boundaries. Generally, collision of two free electrons cannot lead to a change of the collective momentum, but there are special collisions which involve the atomic lattice, so that the sum of electrons' momenta is not conserved after collisions. Such electron-electron-lattice collisions can also lead to damping. If the damping rate is small compared to the plasma frequency, then the real part of permittivity becomes

negative at certain frequencies below the plasma frequency. The transition frequency depends on the background permittivity. Negative real permittivity is an important property of metals that can be utilized to obtain strong reflection in general, but also hyperbolic metamaterials and plasmonic resonances.

Three types of structured media are considered (Figure 1): metamaterials, photonic crystals, and disordered media. Different methods are used to consider reflection from these structures. In metamaterials the structured medium has feature sizes much smaller than the wavelength and thus can be approximated by an effective permittivity. Photonic crystals are periodically structured media with lattice constant a comparable to the half wavelength of incident light $\lambda/2$ where propagating fields can be described by Bloch modes. Disordered media are the most complex case as large representative volumes should be considered. For this case two approximations are available: scattering by single particles (e.g., Mie scattering on spherical particles) or first order Born approximation for weakly scattering structures (such as used in X-ray scattering). In a scattering particle approximation, the interaction between the particles can be reduced neglected if particles are far apart and scattering is weak. We concentrate here on first order scattering approximation as it allows to consider large volumes of densely packed structured media.

The simplest metamaterial is a multilayer out of two materials with varying thickness. Such metamaterial forms a uniaxial medium with optical axis along the direction orthogonal to the layers. Along the optical axis light propagates with an ordinary refractive index independent of polarization. The effective permittivity can be calculated as:

$$\varepsilon_{eff} = \langle \varepsilon \rangle = \frac{\langle D \rangle}{\langle E \rangle} = \frac{D_1 f_1 + D_2 f_2}{E_1 f_1 + E_2 f_2} \tag{5}$$

As layers are much smaller than the wavelength, the electric and displacement fields in each layer can be assumed to be constant. For in-pane polarization the electric field is continuous at the interfaces and thus is constant everywhere $E_1 = E_2$. Thus, the effective permittivity can be obtained as:

$$\varepsilon_{||} = \frac{\varepsilon_1 E_1 f_1 + \varepsilon_2 E_2 f_2}{E_1 f_1 + E_2 f_2} = \varepsilon_1 f_1 + \varepsilon_2 f_2 \tag{6}$$

Which is just the weighted average of the constituting permittivities. For polarization orthogonal to the layers the displacement field is continuous at the boundaries and thus constant in all layers. The permittivity is then:

$$\varepsilon_{\perp} = \frac{D_1 f_1 + D_2 f_2}{D_1 \varepsilon_1^{-1} f_1 + D_2 \varepsilon_2^{-1} f_2} = \frac{1}{\varepsilon_1^{-1} f_1 + \varepsilon_2^{-1} f_2} \tag{7}$$

Which is the inverse average of the permittivities. For wire and sphere media the equation becomes more complex as electric fields become position dependent. But for the case of small filling fraction, where inclusions do not strongly interact with each other, the field in the sphere and cylindrical wire is constant with known factor above the excitation field and outside the cylinder can be assumed to be on average equal to the excitation field. Thus, analytical expressions still can be obtained, which constitute the Maxwell Garnett effective medium approximation.

The uniaxially anisotropic effective medium can be described by a direction dependent wavenumber for the extraordinary wave. When the z direction is chosen along the optical axis then following equation is applied to calculate the wavevector:

$$\frac{k_x^2}{\varepsilon_\perp}+\frac{k_y^2}{\varepsilon_\perp}+\frac{k_z^2}{\varepsilon_{||}}=\frac{\omega^2}{c^2} \tag{8}$$

which describes a surface in k space, so called equifrequency contour.

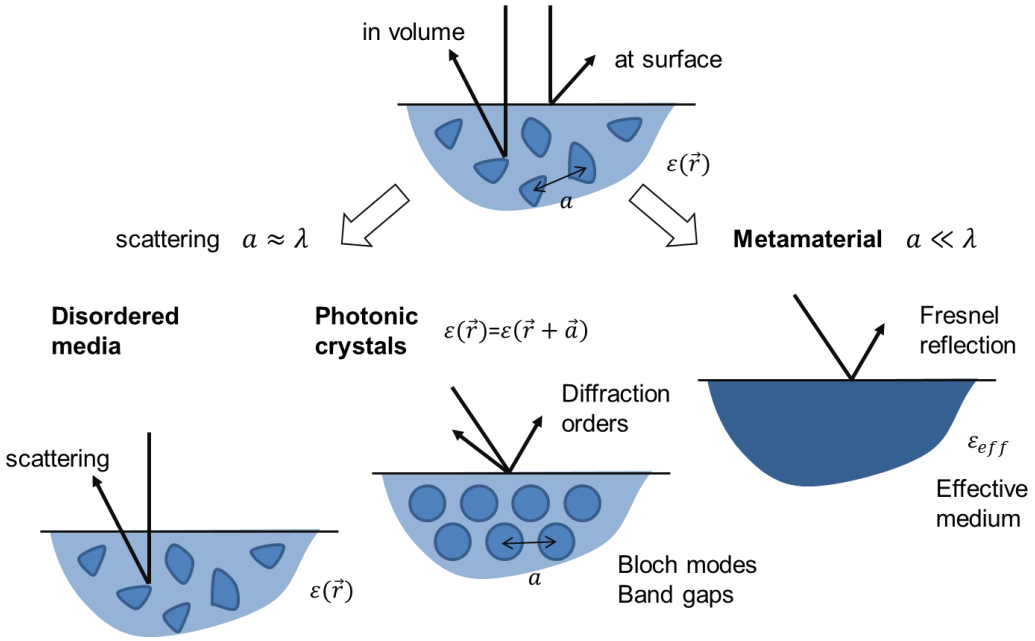

Figure 1: The schematic diagram represents the structured media considered in this work. The reflection from a structured medium can occur at the interface or be accumulated via scattering in the medium. Here we differentiate between media with structural parameters comparable to wavelength and much smaller than the wavelength, so called metamaterials. For the first group we considered disordered media and photonic crystals. Disordered media are described by scattering. Photonic crystal structures are described by their Bloch mode and band gaps. The metamaterials are described by effective medium parameters, allowing the application of Fresnel equations at the interface.

Metamaterials out of dielectric media the equifrequency contour is elliptic. Strong ellipticity can be achieved by combination of dielectric materials with strongly different refractive index, like silicon 3.5 and silica 1.45. But especially striking is the combination of metal and dielectric as the negative permittivity of metal leads to a hyperbolic equifrequency contour that have branches where wavenumbers become infinite [1]. That has strong implications on light focusing inside these media, as very short effective wavelengths and thus almost infinite resolution is available. Also diverging equifrequency contour with infinite area results in infinite density of states in such media leading to very efficient acceptance of radiation.

The reflection from the metamaterial can be calculated with the Fresnel equations using effective medium parameters. It should be mentioned that typical metamaterials have structural features that are only several times smaller than the wavelength. In this case higher order parameters, like effective magnetic response, might be required to correctly describe the effective medium [2]. Also, the exact structure at the boundary becomes important. Thus, effective medium parameters can be used to design structures, but exact reflection should be confirmed with full wave simulations.

A wavevector diagram can be used to construct the direction of light propagation in the metamaterial (Figure 2). The tangential component of the incident reflected and transmitted wavevectors should be equal to allow phase matching at the boundary. Knowing the equifrequency contours and the phase matching condition the transmitted and reflected wavevector can be constructed. Wavevectors define the direction of phase velocity. The group velocity in the medium has a direction orthogonal to the equifrequency contour, which can have a different direction as phase velocity. Strong ellipticity can be used, for example, to collimate the incident divergent beam as in Figure 2 a. In hyperbolic media, depending on the hyperboloid orientation, the incident radiation can be reflected for all incident angles as in Figure 2 b. Also, the modes excited in a hyperbolic medium cannot exit and experience total internal reflection at the boundary. These properties were utilized in our metamaterial emitter for thermophotovoltaics.

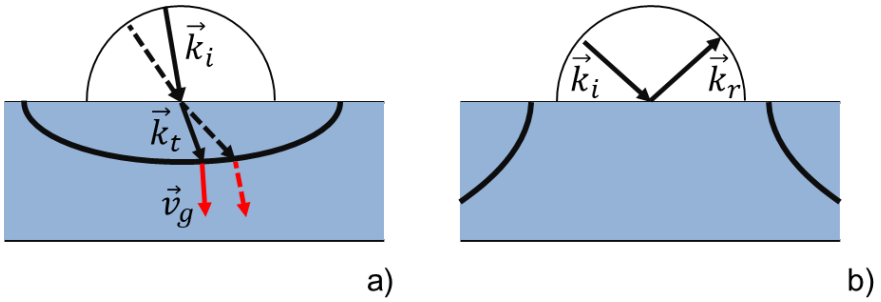

Figure 2: Schematic wavevector diagram for light at boundary between vacuum and anisotropic medium. a) Boundary to dielectric metamaterial with elliptic equifrequency contour. b) Boundary to hyperbolic medium with optical axis vertical to the boundary. No transmission is possible.

If the structural features are increased to approximately half wavelength and the structure is periodic, then a so-called photonic crystal is obtained [3]. Light propagation in periodic systems is described by Bloch modes which are eigen solutions of the electromagnetic wave equation in a unit cell with periodic boundaries. Like for electrons in periodic atomic lattices, a band diagram can be discussed for the electromagnetic waves in media with periodic refractive index. In Figure 3 the schematic band diagram and equifrequency contour of a square lattice photonic crystal is presented. The photonic crystal shows a band gap at frequency ω_2 in the direction ΓX. As can be seen in Figure 3c there are no modes in this direction for this frequency. At the same time the propagation in other directions might be possible, for example, in ΓM direction. Also, complete photonic band gaps can be obtained if directional band gaps overlap. In this case, light is reflected from photonic crystal for any angle of incidence and, in some definitions, for any polarization. The equifrequency contours in photonic crystals can strongly deviate from circles and thus lead to complex refraction of light and direction dependent reflection.

If the wavelength is in the order of the feature size and there is no periodicity, then the exact description of the medium becomes difficult and will require brute force simulations. Two approximations are possible: scattering by weakly interacting particles or Born approximation for weakly scattering structures. If positions of identical scatterers are uncorrelated and they are away from each other, then their scattering profile is proportional to the scattering of a single scatter. Particles with spherical geometry can be described by Mie scattering theory [4]. The inner structure of the particle can lead to spectrally and directionally selective scattering [5]. In this work we mostly concentrate on the first order Born

approximation as it can take both into account, position of the scatterers and their geometry. The approximation can be applied only for structures with small refractive index contrast, so that the incident wave is only weakly scattered. Still the theory has shown good predictive strength even for the refractive index contrast $n_1 - n_2$ more than 1 [P5].

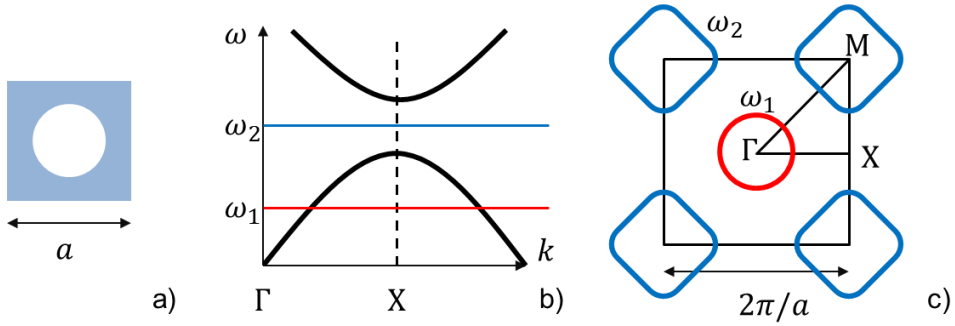

Figure 3: a) Periodic unit cell of a photonic crystal with period a. b) Schematic band diagram for the wavevector in the direction of ΓX. c) Schematic equifrequency contours for frequency ω_1 (red color) and ω_2 (blue color). The square Brillouin zone is shown by black line.

Much of my work on scattering in ordered and disordered media is based on first order approximation and, in particular, on application of Ewald sphere construction for prediction of scattering directions. I would like to introduce here an alternative explanation for Ewald sphere construction that goes slightly beyond the detail level used for discussion of other topics in this background section. Still, I hope it might help to understand the appearance of Ewald sphere from a slightly different perspective.

The scattering predicted by the first order Born approximation can be visualized with help of an Ewald sphere construction in reciprocal space that is known from X-ray diffraction. The Ewald sphere highlights the directions in reciprocal space for which the Bragg condition is fulfilled in the structure. The Fourier transform of the permittivity perturbation $\Delta\varepsilon(\vec{h})$ is used to identify periodicities available in the structure, where $\vec{h}$ is the vector of reciprocal space. The Ewald sphere has a radius equal to absolute value of the scattered wavevector k, and a center position shifted from the center of reciprocal space by negative incident wavevector $-\vec{k}_0$ (Figure 4). In the cases considered in this work $k_0 = k$ as light is scattered elastically and propagates in the same medium as the incident light. Scattering directions are identified by the wavevectors starting from the center of the Ewald sphere and directed towards intersections of the Ewald sphere with $\Delta\varepsilon(\vec{h})$.

A derivation of the Ewald sphere can be obtained using Fourier analysis of scattered field. A scalar analysis is presented here; a vectorial derivation was done by us as supplementary information to publication [P4]. The incident electric field $E_0 \exp i\vec{k}_0\vec{r}$ excites an excess polarization at a permittivity perturbation $\Delta\varepsilon$ which on their side emit light as point sources with electric fields described by a Green's function $G(\vec{r})$. Thus, the scattered field $E_s(\vec{r})$ represent the convolution of excited point source distribution with the Green's function:

$$E_s(\vec{r}) \sim \left(\Delta\varepsilon(\vec{r}) \cdot E_0 e^{i\vec{k}_0\vec{r}}\right) * G(\vec{r}) \tag{9}$$

where the term in the brackets is the excess polarization. The Fourier transform of the electric field will give information about excited directions, where multiplication will convert to convolution and convolution to multiplication:

$$E_s(\vec{h}') \sim \left(\Delta\varepsilon(\vec{h}') * E_0\delta(\vec{h}' - \vec{k}_0)\right) \cdot G(\vec{h}') \sim E_0\Delta\varepsilon(\vec{h}' - \vec{k}_0) \cdot G(\vec{h}') \tag{10}$$

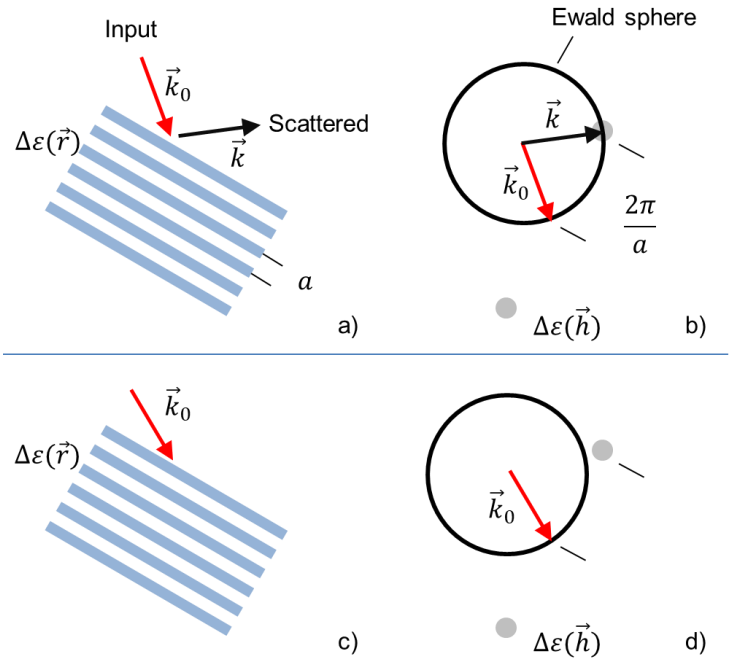

Figure 4: a,c) Schematic figure of the sinusoidal perturbation of permittivity $\Delta\varepsilon(\vec{r})$ and the incident $\vec{k}_0$ (red) and reflected $\vec{k}$ (black) wavevector. b,d) Ewald sphere construction in reciprocal space. The Fourier transform of the permittivity $\Delta\varepsilon(\vec{h})$ (grey) and Ewald sphere (black circle). Scattering in the direction of the intersection between the Ewald sphere and $\Delta\varepsilon(\vec{h})$. Bragg condition is fulfilled in case a,b and not fulfilled in case c,d.

The phase term of the incoming wave results in the convolution with a delta function shifted by $\vec{k}_0$ from the center of reciprocal space, that basically shifts the Fourier transform of permittivity. To avoid shifts of the permittivity function in reciprocal space depending on incident wave direction, the shift is usually attributed to the Green's function by a coordinate system shift $\vec{h} = \vec{h}' - \vec{k}_0$:

$$E(\vec{h}) \sim E_0\Delta\varepsilon(\vec{h}) \cdot G(\vec{h} + \vec{k}_0) \tag{11}$$

Thus, the Green's function is shifted with $-\vec{k}_0$. The point source in a scalar approximation is presented by a spherical wave $G(\vec{r}) = \frac{e^{ikr}}{r} = \frac{\cos kr}{r} + i\frac{\sin kr}{r}$. In reciprocal space it is equal to [6]:

$$G(\vec{h}') = \frac{4\pi}{h'^2 - k^2} + i\frac{2\pi^2}{k}\delta(h' - k) \tag{12}$$

The same as for the Fourier transform of a Heaviside function for a 1D source, there is a delta function and a reciprocal function, both diverging at $h' = k$. The Green's function contains both near and far field contributions. To get an understanding of the far field contribution we can add an incoming spherical wave $-\frac{e^{-ikr}}{r}$ that also diverges in the origin and compensates the divergent real part of the Green's

function. The resulting field is represented by function $\frac{2i\sin kr}{r}$. The constructed field does not have a diverging evanescent field at the origin anymore. There is only a propagating field which is focused in the origin and expands again as an outcoming wave. It has outcoming field and power equal to that of our original Green's function. Its Fourier transform is $i\frac{4\pi^2}{k}\delta(h'-k)$. Thus, the far field of a point source in reciprocal space can be represented by a sphere which can be interpreted as an Ewald sphere. It can be shown that the amplitude of directional plane waves directly corresponds to power scattered in this direction. The full scattered power P is the integral on a spherical surface in reciprocal space [P5]:

$$P = I_0 \frac{\omega^4}{16\pi^2 k^2 c^4} \int_{ESS} \left|\Delta\varepsilon(\vec{h})\right|^2 d\vec{h} \tag{13}$$

where I_0 is the incident intensity and ESS is the Ewald sphere surface.

Thus, scattering from any small refractive index perturbation can be calculated. There are two important assumptions of the first order approximation. First is that $\Delta\varepsilon/\varepsilon$ is small, which is an obvious term as perturbation should be small [P4]. And the second is that the overall change of the incident wave is small, which concerns the amplitude and the phase. Strong incident wave attenuation can be still considered by calculating small, first order, scattering per small representative volume and reducing power of incident wave that enters next small volume. This is possible only if permittivity perturbation has no long-range order along the propagation direction and scattered powers can be added and not the amplitudes. If long range order is involved, then special approaches are required, like coupled wave equations [7], or brute force simulations. The Ewald sphere can still visualize which directions will be coupled but cannot give quantitative results on the scattered power. We have applied first order approximation to disordered arrangement of closely packed spherical particles [P5], so called photonic glass, but also to photonic crystals and quasicrystal structures [P4] with finite thickness.

3. Publications

In this work 14 publications are reviewed where I made a significant contribution in recent years. These publications have also initiated many related contributions, which are listed after the discussion of each of the papers but are not discussed in detail. For each of the 14 publications a short description of the main result is given with explanations that often go beyond the abstract of the work and hopefully provide a helpful insight. It is refrained from the state-of-the-art discussion with corresponding references as this is done in the introduction of each publication itself and given the width of the topic would make the text unnecessarily long.

Here is the list of the topics, structures and papers discussed here:

Broadband omnidirectional reflection

2D photonic crystal

[P1] L. S. Fohrmann, G. Sommer, G. Pitruzzello, T. F. Krauss, A. Yu. Petrov, and M. Eich, "Integrating cell on chip—Novel waveguide platform employing ultra-long optical paths," APL Photonics 2, 96102 (2017).

Multistack opals

[P2] H. S. Lee, R. Kubrin, R. Zierold, A. Yu. Petrov, K. Nielsch, G. A. Schneider, and M. Eich, "Thermal radiation transmission and reflection properties of ceramic 3D photonic crystals," J. Opt. Soc. Am. B 29, 450 (2012).

Photonic glass

[P3] P. N. Dyachenko, J. J. do Rosário, E. W. Leib, A. Yu. Petrov, R. Kubrin, G. A. Schneider, H. Weller, T. Vossmeyer, and M. Eich, "Ceramic photonic glass for broadband omnidirectional reflection," ACS Photonics 1, 1127–1133 (2014).

Spectrally selective omnidirectional reflection

Holographic structures

[P4] L. Maiwald, S. Lang, D. Jalas, H. Renner, A. Yu. Petrov, and M. Eich, "Ewald sphere construction for structural colors," Opt. Express 26, 11352–11365 (2018).

Photonic glass

[P5] G. Shang, L. Maiwald, H. Renner, D. Jalas, M. Dosta, S. Heinrich, A. Yu. Petrov, and M. Eich, "Photonic glass for high contrast structural color," Sci. Rep. 8, 7804 (2018).

2D photonic crystal

[P6] A. E. Serebryannikov, A. Yu. Petrov, and E. Ozbay, "Toward photonic crystal based spatial filters with wide angle ranges of total transmission," Appl. Phys. Lett. 94, 181101–181103 (2009).

Suppressed reflection for selective absorption

Monolayers of spheres on metal

[P7] P. N. Dyachenko, J. J. do Rosário, E. W. Leib, A. Yu. Petrov, M. Störmer, H. Weller, T. Vossmeyer, G. A. Schneider, and M. Eich, "Tungsten band edge absorber/emitter based on a monolayer of ceramic microspheres," Opt. Express 23, A1236 (2015).

Layered metamaterial

[P8] S. Lang, H. S. Lee, A. Yu. Petrov, M. Stormer, M. Ritter, and M. Eich, "Gold-silicon metamaterial with hyperbolic transition in near infrared," Appl. Phys. Lett. 103, 21905–4 (2013).

Layered metamaterial

[P9] P. N. Dyachenko, S. Molesky, A. Yu. Petrov, M. Stormer, T. Krekeler, S. Lang, M. Ritter, Z. Jacob, and M. Eich, "Controlling thermal emission with refractory epsilon-near-zero metamaterials via topological transitions," Nat. Commun. 7, 1–8 (2016).

Broadband absorption

Nanoporous gold

[P10] D. Jalas, R. Canchi, A. Yu. Petrov, S. Lang, L. Shao, J. Weissmüller, and M. Eich, "Effective medium model for the spectral properties of nanoporous gold in the visible," Appl. Phys. Lett. 105, 241906 (2014).

Nanoporous gold

[P11] D. Jalas, L.-H. Shao, R. Canchi, T. Okuma, S. Lang, A. Yu. Petrov, J. Weissmüller, and M. Eich, "Electrochemical tuning of the optical properties of nanoporous gold," Sci. Rep. 7, 44139 (2017).

Reflection from a moving front

Waveguide in a photonic crystal

[P12] M. Castellanos Muñoz, A. Yu. Petrov, L. O'Faolain, J. Li, T. F. Krauss, and M. Eich, "Optically induced indirect photonic transitions in a slow light photonic crystal waveguide," Phys. Rev. Lett. 112, 53904 (2014).

1D Bragg stack

[P13] E. A. Ulchenko, D. Jalas, A. Yu. Petrov, M. Castellanos Munoz, S. Lang, and M. Eich, "Pulse compression and broadening by reflection from a moving front of a photonic crystal," Opt. Express 22, 13280–13287 (2014).

Waveguide in a photonic crystal

[P14] M. A. Gaafar, D. Jalas, L. O'Faolain, J. Li, T. F. Krauss, A. Yu. Petrov, and M. Eich, "Reflection from a free carrier front via an intraband indirect photonic transition," Nat. Commun. 9, 1447 (2018).

4. Discussion

4.1. Broadband omnidirectional reflection

[P1] L. S. Fohrmann, G. Sommer, G. Pitruzzello, T. F. Krauss, A. Yu. Petrov, and M. Eich, "Integrating cell on chip—Novel waveguide platform employing ultra-long optical paths," APL Photonics 2, 96102 (2017).

My contribution was the idea of the 2D integrating cell, the supervision of theoretical calculations, simulations and characterization, input to the publication.

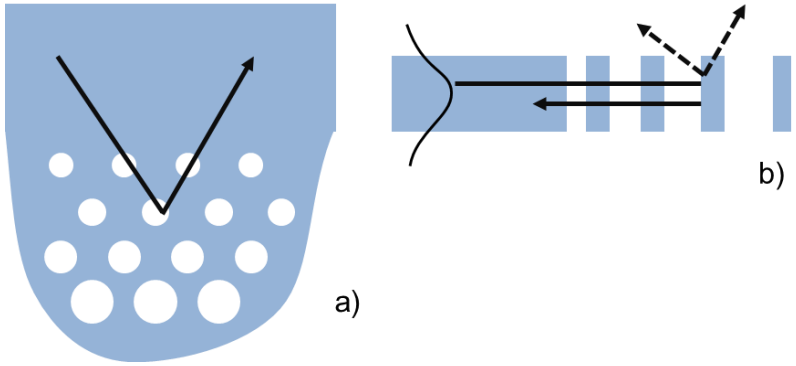

Figure 5: Schematic representation of 2D photonic crystal reflector with adiabatic transition. a) Top view showing the reflection of incident light at the tapered photonic crystal reflector made of cylindrical holes in silicon slab. b) Side view which shows the schematic guided mode profile in a slab waveguide. Upon reflection from photonic crystal reflector the vertical scattering is a problem (dashed lines).

The main task of this work was to design a special reflector for a 2D integrating cell. The 3D integrating cells (spheres) are well known where light is confined by multiple reflections within a spherical volume. The reflection factor defines how many reflections light can accumulate until it decays to 1/e intensity. The best reflectors in 3D integrating cells show reflectivity of 99% and thus 100 reflections before 1/e decay. In 2D integrating optics there is also a goal to keep light for long time on chip to, e.g., increase interaction with environment by evanescent part of the guided mode. This can be done by long waveguide folded in a meander or spiral shape. But waveguides are produced by lithographic approaches and have intrinsic side wall roughness that leads to accumulation of scattering in long waveguides. In this publication a 2D integrating cell was proposed as an alternative route to achieve long propagation length on chip. For that light is kept within a defined area of a slab waveguide by special in-plane reflectors. The reflectors should reflect incident light back into the slab mode. The additional complication of such reflectors compared to 3D case is that they not only should not transmit or absorb light but also, they should prevent vertical scattering of light out of the slab plane. This additional condition is the main issue that was tackled in the publication.

As a first design a 2D photonic crystal with hexagonal array of holes in silicon slab was investigated as reflector. It is known that such photonic crystals open a complete photonic band gap and thus can block transmission of light in any in-plane direction. At the same time the vertical scattering at the transition from unstructured slab into photonic crystal region leads to reflection in the order of 98%. In the work an

adiabatic taper was developed to increase the reflectivity to 99%. The 25 cm propagation length was demonstrated in a chip area with 1.8 mm diameter.

Due to the large propagation length in the integrating cell the light becomes sensitive to the small variations in the absorption, which can be used e.g., for gas sensing. This sensitivity was experimentally used to track the free carrier concentration and decay time in silicon slab illuminated by visible light:

L. S. Fohrmann, N. Lotfi, B. Alzein, M. A. Gaafar, A. Yu. Petrov, and M. Eich, "Free-carrier detection in a silicon slab via absorption measurement in 2D integrating cells," Opt. Lett. 44, 175 (2018).

[P2] H. S. Lee, R. Kubrin, R. Zierold, A. Yu. Petrov, K. Nielsch, G. A. Schneider, and M. Eich, "Thermal radiation transmission and reflection properties of ceramic 3D photonic crystals," J. Opt. Soc. Am. B 29, 450 (2012).

My contribution was the supervision of theoretical calculations and simulations, input to the publication.

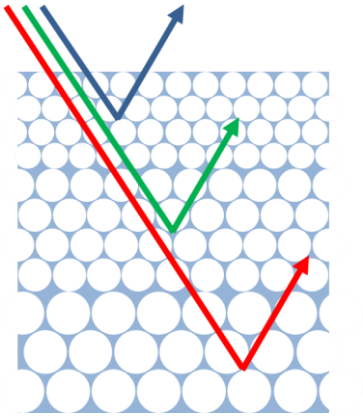

Figure 6: Schematic representation of the multistack opal for broadband reflection which reflects different wavelengths in different stacks of opal.

The reflection of thermal radiation requires extra broadband reflectivity. Particularly for the hot gas environment in turbine applications the reflectivity should span the wavelength range from 1 to 5 µm. Such bandwidth cannot be covered by a complete photonic band gap of a 3D photonic crystal out of high temperature stable ceramic materials. Thus, for this application a concept of multistack photonic crystal was developed. As a photonic crystal a face centered cubic packing of monodisperse spherical particles was considered, so called opal. It was shown that an inverse opal from yttria stabilized zirconia, which is obtained by infiltration of polystyrene opal and removal of polystyrene, with refractive index of 2.1 can block up to 15% of the relative bandwidth $\Delta\lambda/\lambda$ in one direction. To block radiation from 1 to 5 µm 10 stacks with varying particle size and total thickness of approximately 100 µm are required. This way the band gaps of individual opal stacks overlap and allow a broadband response. At the same time the band gap frequency of each stack is dependent on the angle of incident radiation. But the band gaps of all opal stacks shift the same way, thus the broadband reflectivity is maintained even at oblique incidences. Hemispherical reflectance larger the 80% was predicted.

The concept was the followed by deposition of double and triple stack opals:

R. Kubrin, H. S. Lee, R. Zierold, A. Yu. Petrov, R. Janssen, K. Nielsch, M. Eich, and G. A. Schneider, "Stacking of ceramic inverse opals with different lattice constants," J. Am. Ceram. Soc. 95, 2226–2235

H. S. Lee, R. Kubrin, R. Zierold, A. Yu. Petrov, K. Nielsch, G. A. Schneider, and M. Eich, "Photonic properties of titania inverse opal heterostructures," Opt. Mater. Express 3, 1007–1019 (2013).

R. Kubrin, R. M. Pasquarelli, M. Waleczek, H. S. Lee, R. Zierold, J. J. do Rosário, P. N. Dyachenko, Montero Moreno, Josep M., A. Yu. Petrov, R. Janssen, M. Eich, K. Nielsch, and G. A. Schneider, "Bottom-up fabrication of multilayer stacks of 3D photonic crystals from titanium dioxide," ACS Appl. Mater. Interfaces 8, 10466–10476 (2016).

[P3] P. N. Dyachenko, J. J. do Rosário, E. W. Leib, A. Yu. Petrov, R. Kubrin, G. A. Schneider, H. Weller, T. Vossmeyer, and M. Eich, "Ceramic photonic glass for broadband omnidirectional reflection," ACS Photonics 1, 1127–1133 (2014).

My contribution was the supervision of simulations and characterization, input to the publication.

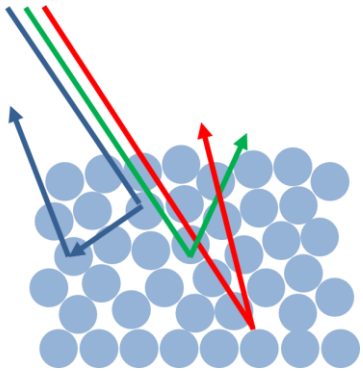

Figure 7: The schematic presentation of light reflected from direct photonic glass. Broadband reflection is achieved where long wavelength light (red) has longer penetration depth.

The broadband reflection of light can be achieved with disordered structures. But the structural unit a should be still adjusted to the wavelength of incident light to provide efficient scattering. It was shown that a disordered arrangement of spherical particles, so called photonic glass, with 3 µm diameter can efficiently reflect light in the spectral region of thermal radiation between 1 and 6 µm. Larger particles will have fewer scattering surfaces per coating thickness and smaller particles will insufficiently scatter long wavelength radiation, which would go through the photonic glass as through an effective medium with an average index. It was shown that light reflected from such a disordered structure has a transmission described by the diffusion equation. Namely, the transmission is inversely proportional to the material thickness. It was shown that 80 µm of such a coating can reflect 80% of the incident thermal radiation which is a strong improvement in comparison to conventional thermal barrier coatings.

The developed approach for photonic glass-based reflectors was later used to demonstrate inverse photonic glass out of yttria stabilized zirconia:

J. J. do Rosario, P. N. Dyachenko, R. Kubrin, R. M. Pasquarelli, A. Yu. Petrov, M. Eich, and G. A. Schneider, "Facile deposition of YSZ-inverse photonic glass films," ACS Appl. Mater. Interfaces 6, 12335–12345 (2014).

The high temperature stable photonic glass was obtained also directly from yttria stabilized zirconia particles which showed stability up to 1400 °C:

E. W. Leib, R. M. Pasquarelli, J. Do Rosário, P. N. Dyachenko, S. Döring, A. Puchert, A. Yu. Petrov, M. Eich, G. A. G. A. Schneider, R. Janssen, H. Weller, T. Vossmeyer, Yttria-stabilized zirconia microspheres: Novel building blocks for high-temperature photonics. J. Mater. Chem. C. 4, 62–74 (2015).

Apart from broadband reflectivity direct photonic glass has very small thermal conductivity due to small contact areas between particles, which we confirmed experimentally:

G. Shang, P. Dyachenko, E. W. Leib, T. Vossmeyer, A. Yu. Petrov, and M. Eich, "Conductive and radiative heat transfer inhibition in YSZ photonic glass," Ceram. Int. 46, 19241 (2020).

4.2. Selective reflection

[P4] L. Maiwald, S. Lang, D. Jalas, H. Renner, A. Yu. Petrov, and M. Eich, "Ewald sphere construction for structural colors," Opt. Express 26, 11352–11365 (2018).

My contribution was the idea of Ewald sphere application for scattering description and the algorithm for structure generation, supervision of theoretical calculations and simulations, input to the publication.

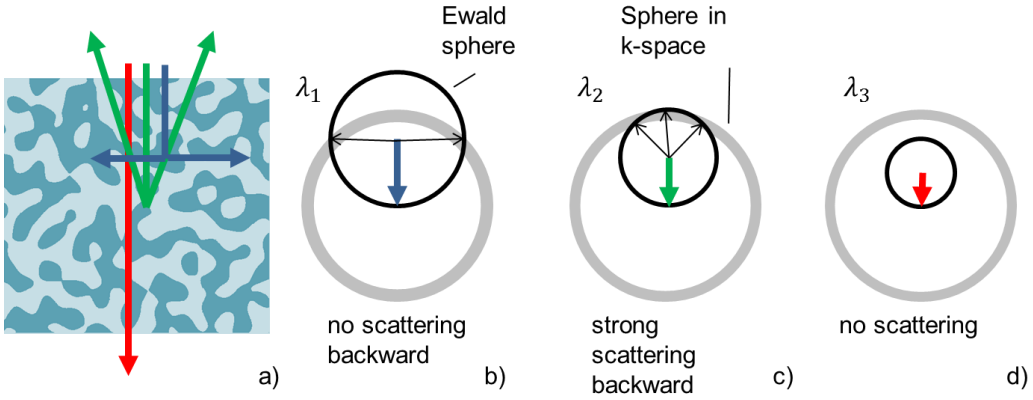

Figure 8: The schematic presentation of light reflection in the medium with long range order and no directional order. a) dielectric constant distribution. b,c,d) Ewald sphere construction in reciprocal space, k-space, for light scattering at three wavelengths. The Fourier transform of the dielectric constant distribution is a spherical shell, represented by the grey circle. Thus, equal periodicities are available in all directions inside this material. The Ewald sphere construction shows strong backscattering only for the case when the Ewald sphere touches the k-shell of the dielectric function (case c).

In the frame of this work several important contributions were developed. First, a novel disordered material was proposed with long range order and absence of directional selectivity. Such material is mathematically described by a sum of sinusoidal functions with equal period and amplitude, but random orientation and phase. The final sum is binarized by a sign function to represent a bicontinuous network of two media as presented in Figure 8 a. When the number of sinusoidal functions is approaching infinity, the Fourier transform of the binarized structure is represented by the spherical shell in reciprocal space. Such a material is characterized by the long-range order, as the spectral features are sharp in reciprocal space and the shell is thin. At the same time there is no directional order as the same periodicity is available in any direction.

The second contribution is connected to the application of the first order approximation to describe scattering in such structures. Namely, the Ewald sphere construction was used to show that only certain

wavelengths are strongly back scattered and other wavelengths are not scattered at all or scattered in the orthogonal directions and thus are trapped inside the scattering medium via total internal reflection. This directional scattering allows achieving spectral selectivity in a disordered material which is interesting for structural color applications. At the same time, this selectivity is independent of the incident angle of light as the Fourier transform of the dielectric function is a symmetrical spherical shell and the Ewald sphere construction will also show strong backscattering for the same wavelength at other incident angles.

This concept later led us to the development of low refractive index quasiperiodic structures which suppress radiation of light. In any direction light experiences a strong reflection and thus emission of light from a point source is strongly suppressed:

L. Maiwald, T. Sommer, M. S. Sidorenko, R. R. Yafyasov, M. E Mustafa, M. Schulz, M. V. Rybin, M. Eich, A. Yu. Petrov, "Control over Light Emission in Low-Refractive-Index Artificial Materials Inspired by Reciprocal Design," Adv. Opt. Mat., accepted (2021), https://doi.org/10.1002/adom.202100785

[P5] G. Shang, L. Maiwald, H. Renner, D. Jalas, M. Dosta, S. Heinrich, A. Yu. Petrov, and M. Eich, "Photonic glass for high contrast structural color," Sci. Rep. 8, 7804 (2018).

My contribution, together with Hagen Renner, was the idea of a sharp transition via motif optimization, supervision of theoretical calculations and simulations, input to the publication.

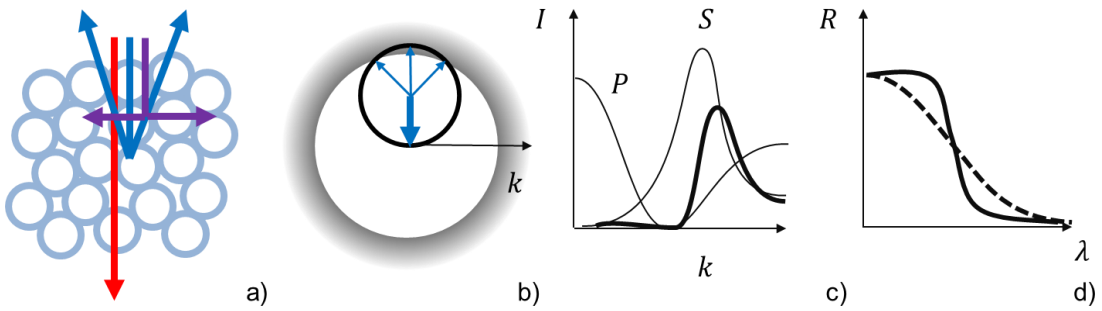

Figure 9: a) Schematic reflection from a hollow sphere photonic glass. Blue light is strongly backscattered, and long wavelength light is transmitted. b) The Fourier transform of the dielectric constant distribution is represented by a spherical function with low intensity in the central region and a sharp transition at larger k vectors. c) This Fourier transform can be obtained by shifting the zero point of the motif Fourier transform (form factor, P) to the left side of the lattice Fourier transform (structure factor, S). d) Such a Fourier transform allows sharp transition in reflection as schematically show by solid black line as compared to full sphere or inverse photonic glass (dashed line).

We have applied the first order approximation to photonic glasses to improve the blue color saturation of structural color effect. The photonic glass shows a transition from no scattering to strong backscattering when the wavelength is reduced and approaches the distance between the particles. This transition is usually quite smooth as shown by the dashed line in the Figure 9 d. Thus, there is also a residual reflection of green and red color which reduces the blue color saturation. The smooth transition has to do with the short-range order, that does not provide a strictly defined periodicity condition. In the presented publication we have managed to optimize the particles (motifs) of photonic glass such that a sharper reflection transition is obtained (solid line in Figure 9 d).

To obtain a sharp transition of scattering the Fourier transform of the photonic glass permittivity distribution should have a sharp transition from small to large wavenumbers in reciprocal space. The Fourier transform of the permittivity is a multiplication of the Fourier transform of the photonic glass lattice, defined by the center points of the spheres, (structure factor) and the Fourier transform of the motif (form factor). We have optimized the motifs in such a way that the zero point of the form factor is closer to the center of reciprocal space than the peak of the structure factor (Figure 9 c). In the full sphere photonic glass, the zero point is on the right side of the structure factor peak. To shift the zero point closer to the center of reciprocal space core shell particle can be used with the permittivity changing non-monotonously from the center of the particle through the shell into the background material. This is also fulfilled for hollow particles presented in Figure 9 a.

Based on this theoretical prediction several experimental structures were realized by us leading to highly saturated blue structural color:

G. Shang, Y. Häntsch, K. P. K. P. Furlan, R. Janßen, G. A. G. A. Schneider, A. Yu. Petrov, M. Eich, "Highly selective photonic glass filter for saturated blue structural color." APL Photonics. 4, 046101 (2019).

Y. Häntsch, G. Shang, A. Yu. Petrov, M. Eich, G. A. Schneider, "YSZ Hollow Sphere Photonic Glasses: Tailoring Optical Properties for Highly Saturated Non-Iridescent Structural Coloration." Adv. Opt. Mater. 7, 1900428 (2019).

G. Shang, M. Eich, and A. Petrov, "Photonic glass based structural color," APL Photonics 5, 060901 (2020).

[P6] A. E. Serebryannikov, A. Yu. Petrov, and E. Ozbay, "Toward photonic crystal based spatial filters with wide angle ranges of total transmission," Appl. Phys. Lett. 94, 181101–181103 (2009).

My contribution was the explanation for broadband Fabry-Perot feature due to the flat equifrequency contour of the photonic crystal, input to the publication.

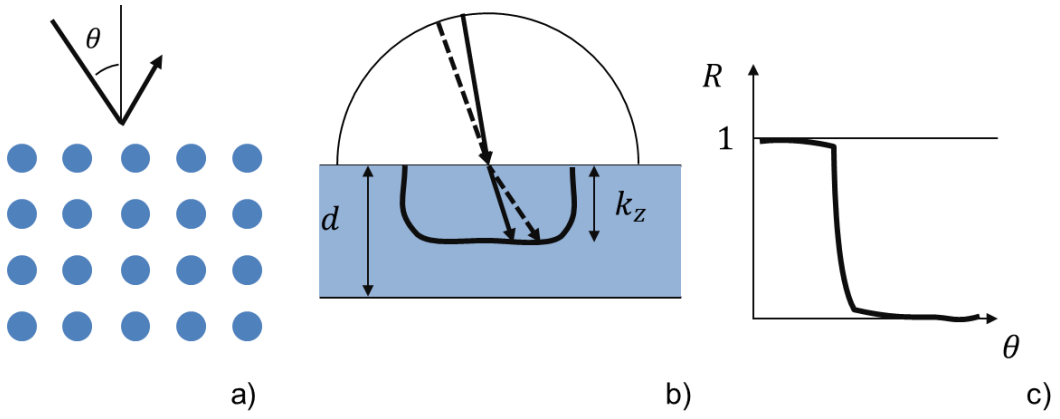

Figure 10: a) Schematic reflection from a square lattice 2D photonic crystal. b) Wavevector diagram inside the photonic crystal is defined by the equifrequency contour (solid line). If the equifrequency contour is flat the z-component of the wavevector k_z in the photonic crystal stays constant independent of the angle of incident light. c) Using such angle independence, a sharp transition in the reflection versus angle can be obtained from reflection 1 to almost 0.

In some applications sharp directional filters are required, so called spatial filter, with sharp transition between wide ranges of total transmission and total reflection (Figure 10 c). Where it is simple to obtain total reflection with photonic crystals by opening a directional band gap, the total transmission in a defined angle range is a non-trivial function. We have utilized the special shape of the equifrequency contour of photonic crystals to obtain such property. Namely the equifrequency contour of square lattice of dielectric rods can be tuned to have square like shape. The light excited from outside follows the phase matching condition at the surface of the photonic crystal and, thus, the tangential component of the wavevector is conserved. The longitudinal component is then given by a particular equifrequency contour. If the equifrequency contour is flat as in Figure 10 b, then the normal component of the wavevector k_z excited in the photonic crystal is a constant for a range of incident angles.

The wavenumber k_z defines the phase that light accumulates when it transmitts through the photonic crystal layer. Transmission close to one through photonic crystal can be obtained if a Fabry-Perot condition is fulfilled, which is $2k_z d = \pi + 2\pi n$. Such a condition is fulfilled in conventional materials only for one angle of incidence. In photonic crystal with adjusted equifrequency contour this condition can be fulfilled for a range of angles, leading to resonant transmission of 1 for a spectrum of angles. In the present publication also condition to obtain total reflection at small and large angles of incidence with a region of total transmission at intermediate angles was mentioned. Such functionality was also discussed later for multifrequency spatial filtering:

A. E. Serebryannikov, E. Colak, A. Yu. Petrov, P. V. Usik, and E. Ozbay, “Multifrequency spatial filtering: A general property of two-dimensional photonic crystals,” Photonic. Nanostruct. 18, 1–9 (2016).

4.3. Suppressed reflection for selective absorption

Metal films are usually considered in the context of optical mirrors due to the high reflectivity of free electrons in metals. The electronic currents induced by light not only produce a reflected wave, but also efficiently screen the incident electric fields and substantially reduce the penetration depth and amplitude of fields inside metal. At the same time, the free electrons in the metal also experience collisions and scatter at defects, phonons and other electrons. These collisions significantly damp the collective motion of electrons and lead to absorption of light. Thus, metals would efficiently absorb light if fields in the metal are excited. In this section we have applied structuring of the metal or combination of metal with dielectric structures to introduce electric fields into the metal and thus decrease reflection and increase absorption at some frequencies. In particular, diluting metal volume [P8, P9, P10] or introducing electric field orthogonal to the metal surface [P7] allowed reducing reflection at designed frequencies. Also changes at the metal-dielectric interface might significantly influence reflection properties [P11]

Spectral selectivity of absorption is important for several applications. First, we should mention that the emission problem is equivalent to absorption problem due to Kirchoff’s law of thermal radiation. Thus, the spectral emissivity of the material is equivalent to its absorptivity. Here, in particular, thermophotovoltaic applications are addressed, where strong thermal emissivity has to be engineered at short wavelengths and no thermal emissivity at long wavelengths. This way the thermal emission of such selective emitters can be converted by photovoltaic cell with defined band gap with photons below the band gap not being excited by the emitter.

[P7] P. N. Dyachenko, J. J. do Rosário, E. W. Leib, A. Y. Petrov, M. Störmer, H. Weller, T. Vossmeyer, G. A. Schneider, and M. Eich, "Tungsten band edge absorber/emitter based on a monolayer of ceramic microspheres," Opt. Express 23, A1236 (2015).

My contribution was the supervision of simulations and characterization, input to the publication.

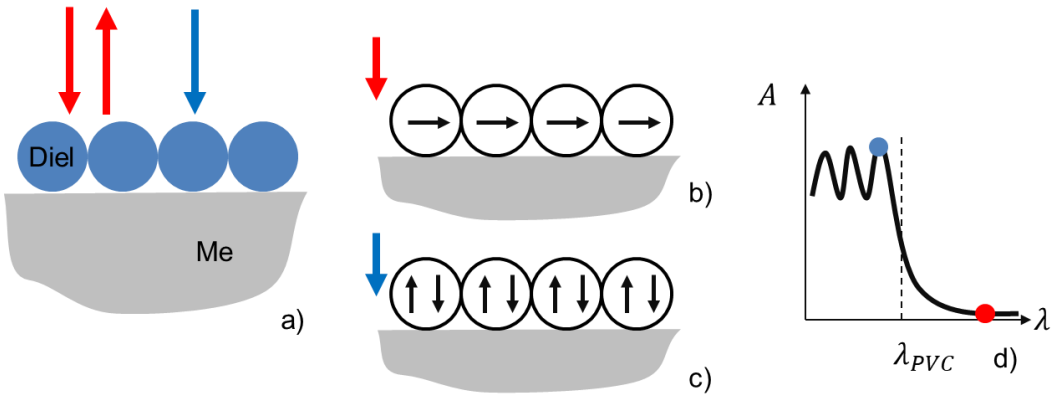

Figure 11: a) Schematic reflection from a metallic substrate coated by a monolayer of dielectric spheres. Long wavelengths light (red) is reflected, and short wavelength light (blue) is absorbed. b) Schematic presentation of electric field orientation in dielectric spheres for long wavelength excitation. Fields are parallel to metal surface. c) Schematic presentation of electric field orientation in dielectric sphere for short wavelength excitation. Fields are orthogonal to metal surface. d) Schematic spectral absorption of the metal substrate with a monolayer of dielectric spheres. At short wavelengths below wavelength of the photovoltaic cell λ_{PVC} resonance absorption is observed due to excitation of multipole resonances inside the dielectric spheres.

The absorption in metals can be initiated by the multipoles excitation in dielectric particles close to the metal surface. We have observed in simulations that certain multipoles introduce electric fields orthogonal to the metal surface. Metal cannot screen such fields efficiently and significant absorption is observed at the wavelengths of multipole resonances. In Figure 11 it is shown that long wavelength light excites mostly modes parallel to the interface, which have almost zero electric field at metal surface and thus do not show significant absorption. In contrast, short wavelength light can also excite multipoles with electric fields orthogonal to the metal surface, such multipoles excitation leads to strong absorption.

To maximize the absorption at the multipole resonance it is important to meet a critical condition between coupling and absorption. The external plane wave is mostly reflected into the backpropagating plane wave and partly excites the resonant modes that accumulate energy with time. These resonant modes can lose energy coupling into the backpropagating plane wave or by absorption in the metal. If coupling and absorption rates are equal, then critical coupling condition is met, where the backpropagating mode is cancelled (the back reflected wave and outcoupled wave have equal amplitudes and opposite phase) and absorption is equal to one. The blue and red color excitation in Figure 11 correspond to short and long wavelength light correspondingly. The concept is not fixed to visible light and the cut off wavelength can be shifted by changing the particle size. Thus, different photovoltaic cells can be addressed. The advantage of this concept is that metal does not have to be structured in this case. This is important for high temperature applications, such as thermophotovoltaics, as structured metals change their shape due to surface diffusion.

The absorption selectivity can be changed from a cut-off characteristic to a narrow maximum. This was obtained by changing to metal-dielectric particles, where the higher order multipoles are suppressed by the metal in the core of the particles:

P. N. Dyachenko, A. Yu. Petrov, and M. Eich, "Perfect narrow-band absorber based on a monolayer of metallodielectric microspheres," Appl. Phys. Lett. 103, 211105 (2013).

[P8] S. Lang, H. S. Lee, A. Yu. Petrov, M. Stormer, M. Ritter, and M. Eich, "Gold-silicon metamaterial with hyperbolic transition in near infrared," Appl. Phys. Lett. 103, 21905 (2013).

My contribution was the idea of shifting the hyperbolic transition to NIR range by combination of metal with high index material, supervision of theoretical calculations, simulations and characterization, input to the publication.

[P9] P. N. Dyachenko, S. Molesky, A. Yu. Petrov, M. Stormer, T. Krekeler, S. Lang, M. Ritter, Z. Jacob, and M. Eich, "Controlling thermal emission with refractory epsilon-near-zero metamaterials via topological transitions," Nat. Commun. 7, 11809 (2016).

My contribution was the supervision of simulations and characterization, input to the publication.

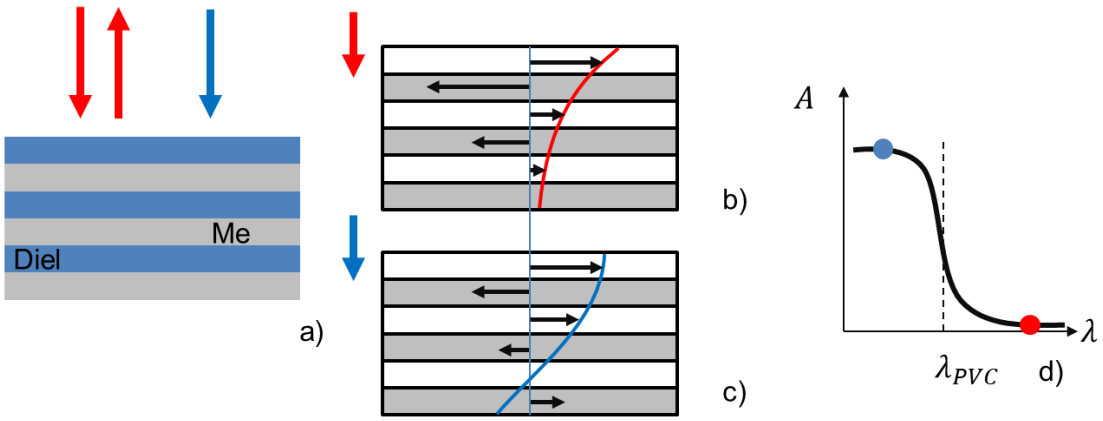

Figure 12: a) Schematic reflection of light at metal-dielectric multilayer metamaterial. b) Schematic displacement field distribution in the layers. The displacement field in the metal is larger than in dielectric, thus metallic reflection prevails, and fields decay exponentially. c) Displacement field in dielectric is larger than in the metal. Thus, metamaterial behaves as a dielectric and the electromagnetic field can penetrate into the material as a sinusoidal wave and eventually gets absorbed. d) spectral selectivity of the multilayer metamaterial absorber.

Another way to let electromagnetic field penetrate the metal is the combination of thin metallic and dielectric layers (Figure 12). The strong negative currents in the metal are compensated by positive displacement currents in dielectric. Depending on the prevalence of the positive or negative displacement field the metamaterial behaves itself as an effective dielectric or metal. In case of overall metallic properties, the exponential decay of the fields is obtained (Figure 12) and light is mostly reflected. In case of overall dielectric properties, the fields are sinusoidal and propagate into the metamaterial (Figure 12). That can lead to significant absorption without reflection.

The dielectric properties of metal are described by bound and free electrons. Free electrons can be approximated by a free electron Drude model, which explains negative permittivity of metals at small frequencies. Due to inertia of electrons the amplitude of electron oscillation in the field reduces quadratically with frequency and at some frequency the displacement of free electrons is insufficient to compensate the dielectric response of bound electrons in the metal. Such transition usually lies in the UV and visible range. The metal-dielectric multilayer allows shifting this transition from dielectric to metallic properties to the NIR range. As the negative permittivity of metals grows quadratically with wavelength high index dielectrics and thicker dielectric layers should be used to shift the transition significantly. We have shown that silicon with refractive index of 3.5 is a good candidate to shift the transition to NIR when combined with gold [P8]. But to allow high temperature applications, refractory metals, e.g. tungsten, should be used. Tungsten has a strong dielectric contribution from its bound electrons and larger collision frequency of free electrons as gold. We could shift the transition to 1.3 μm using hafnia with refractive index of 2.0.

For the thermophotovoltaic application it is important to significantly suppress the long wavelength emission and to approach maximal emissivity at small wavelengths. The absorption at small frequencies is approaching one which is also the property of the metamaterial. Close to the transition the effective refractive index becomes close to one and thus is well matched to air outside of the metamaterials. The light can penetrate the metamaterial without reflection and is absorbed inside. At longer wavelength, the absorptivity in tungsten metamaterials is low but still significant. Later we have shown that thermal annealing of metamaterial can improve metallic properties of tungsten by reducing the collision frequency at grain boundaries:

M. Chirumamilla, G.V Krishnamurthy, K. Knopp, T. Krekeler, M. Graf, D. Jalas, M. Ritter, M. Störmer, A. Yu. Petrov, and M. Eich, “Metamaterial emitter for thermophotovoltaics stable up to 1400 °C,” Sci. Rep. **9**, 7241 (2019).

We have also investigated how the thermal stability can be improved at technical vacuum conditions:

M. Chirumamilla, G.V Krishnamurthy, S. Rout, M. Ritter, M. Störmer, A. Yu. Petrov, and M. Eich, “Thermal stability of tungsten based metamaterial emitter under medium vacuum and inert gas conditions,” Sci. Rep. 10, 3605 (2020).

[P10] D. Jalas, R. Canchi, A. Y. Petrov, S. Lang, L. Shao, J. Weissmüller, and M. Eich, “Effective medium model for the spectral properties of nanoporous gold in the visible,” Appl. Phys. Lett. 105, 241906 (2014).

My contribution was the idea to approximate nanoporous gold by a cubic grid of wires, supervision of theoretical calculations, input to the publication.

Nanoporous gold is a bicontinuous network of gold and pores with variable size of structural elements. When the gold ligament diameters are much smaller than the optical wavelength, then an effective medium description can be applied. Due to the random isotropic structure, it is expected that an isotropic effective permittivity can be defined. To approach this problem, we have considered the nanoporous network as approximately consisting out of cylindrical ligaments. Taking into account that the gold filling fraction was 25-35% in our experiments, we approximated the ligaments to be surrounded by air. We have assumed that excitation electric field on average can be described as to 2/3 being orthogonal to ligaments and to 1/3 parallel to them. A simple orthogonal grid of cylindrical gold wires should thus be a good

approximant for the structure. For the excitation case shown in Figure 13 b the electric field is orthogonal to 2/3 of wires (in plane and out of plane wires) and is parallel to 1/3 of wires (in plane). Neglecting the junction volume and the interaction between orthogonal wires we have applied the Maxwell-Garnett effective medium approximation.

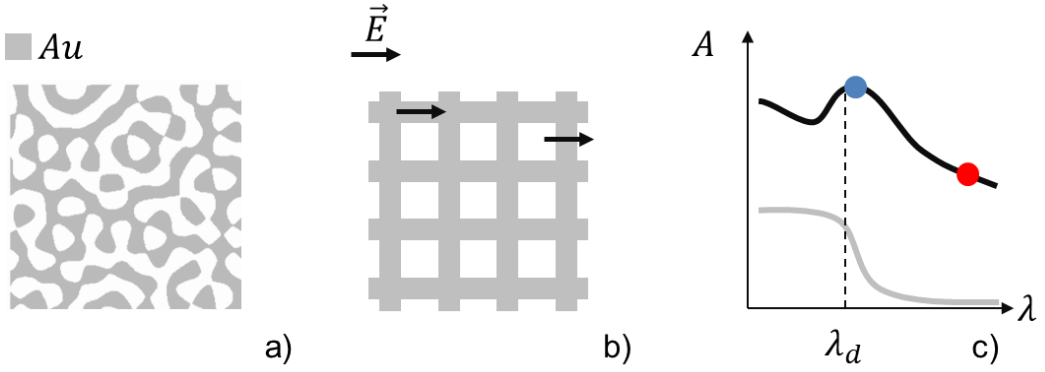

Figure 13: a) A schematic representation of the nanoporous gold structure. An interpenetrating 3D network of gold and pores is obtained. b) An optical structure of nanoporous gold represented by a cubic lattice of gold nanowires. The incident electric field can be split into the contributions parallel to the wires and orthogonal to the wires. c) Schematic absorption spectrum of gold (grey) and nanoporous gold (black). The electric field orthogonal to gold ligaments in nanoporous gold excites a plasmonic resonance at wavelength slightly larger than d-band wavelength λ_d (blue dot). The dilution of gold due to porosity leads to decrease of reflectivity and increase of absorption at longer wavelengths (red dot).

The applied effective medium approximation allowed to explain optical response of nanoporous gold. Generally, the gold response is dictated by the free s-band electrons in long wavelength range and bound d-band electrons at wavelengths below 500 nm. At long wavelengths gold is strongly reflecting, at wavelengths below 500 nm the gold becomes dielectric with strong absorption (see Figure 13 c, grey line). Nanoporosity dilutes gold, making it less reflective. Thus, light can penetrate into gold and experiences stronger absorption. Also, a clear plasmonic resonance can be observed at wavelengths slightly above the plasma wavelength. This is the resonance of plasmonic oscillation in the wires orthogonal to the field. This resonant excitation leads to slightly stronger reflection and absorption of nanoporous gold at the resonance wavelengths.

The presented simplified model allowed to explain spectral features of the nanoporous gold reflection and transmission. At the same time no quantitative correspondence was observed between experiment and theory. Our ongoing research concentrates on the adjustment of the effective medium model to consider finite volume of the junctions and complex geometry of ligaments and to define correct permittivity of gold in small gold ligaments as electrons experience increased collision frequency due to interaction with the surface.

[P11] D. Jalas, L.-H. Shao, R. Canchi, T. Okuma, S. Lang, A. Y. Petrov, J. Weissmüller, and M. Eich, "Electrochemical tuning of the optical properties of nanoporous gold," Sci. Rep. 7, 44139 (2017).

My contribution was the supervision of theoretical calculations, simulations and characterization, and input to the publication.

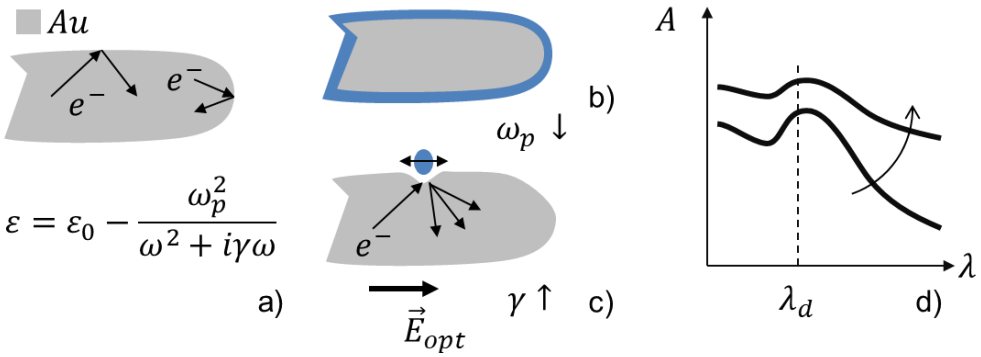

Figure 14: a) Schematic presentation of a gold ligament with paths of free electrons colliding with the surface. The permittivity of gold in a gold ligament is partly defined by s-band electrons with their plasma frequency ω_p and collision frequency γ of electrons. b) Gold ligament with oxidized surface. The oxidation of gold in electrolyte at positive biases leads to a dielectric coating on the gold ligament (blue) and effectively less free electrons and smaller plasma frequency of the gold ligament. c) Schematic presentation of the adsorbates at the surface of gold (blue). The adsorbates can change the effective collision frequency of electrons due to temporal electron transfer into the adsorbate state or due to effective surface roughness induced by the adsorbate. d) Due to both effects, decrease of the plasma frequency and increase of the collision frequency the absorption of nanoporous gold can significantly increase. The change can be induced electrochemically.

The optical properties of gold in the ligaments of nanoporous gold are strongly influenced by the surface. The surface modification can be also used to tune the optical response. Electrochemical surface oxidation was used to significantly increase absorption of nanoporous gold. In this case the surface oxidation leads to reduction of free electrons available for the interaction with optical field. Effectively, it can be considered as reduction of the effective plasma frequency. We have shown that at 1V of applied bias the effect is sufficient to change the transmission through 100 nm thick nanoporous gold sample by 30%.

Apart from change in plasma frequency, we are currently investigating the effect surface modification on the collision frequency as well. It is expected that adsorbates on the surface of gold ligaments can also change the effective collision frequency of free electrons. Two mechanisms are discussed: temporal electron transfer and effective surface roughness. In case of transfer, the electron temporally populates the adsorbate state and effectively increases a probability to absorb a photon (Figure 14 c). Also, the adsorbate can change the potential at the metal interface and this way provides effective roughness of the surface for electron scattering, which influences the effective collision frequency leading to absorption (Figure 14 b).

The size of the ligaments and, thus, surface to volume ratio, plays a crucial role in the surface driven effects. We have also observed that smaller ligament size leads to increase in collision frequency and with that increase in the absorption of nanoporous gold:

M. Graf, D. Jalas, J. Weissmüller, A. Yu. Petrov, and M. Eich, “Surface-to-Volume Ratio Drives Photoelectron Injection from Nanoscale Gold into Electrolyte,” ACS Catal. 9, 3366 (2019).

We have also estimated the possible effect of adsorbates on collision frequency theoretically:

J. B. Khurgin, A. Yu. Petrov, M. Eich, and A. V. Uskov, "Direct Plasmonic Excitation of the Hybridized Surface States in Metal Nanoparticles," ACS Photonics 8, 2041 (2021).

4.4. Reflection from a moving front

[P12] M. Castellanos Muñoz, A. Yu. Petrov, L. O'Faolain, J. Li, T. F. Krauss, and M. Eich, "Optically Induced Indirect Photonic Transitions in a Slow Light Photonic Crystal Waveguide," Phys. Rev. Lett. 112, 53904 (2014).

My contribution was the idea to describe interaction with a front as an indirect transition, supervision of theoretical calculations, simulations and characterization, input to the publication.

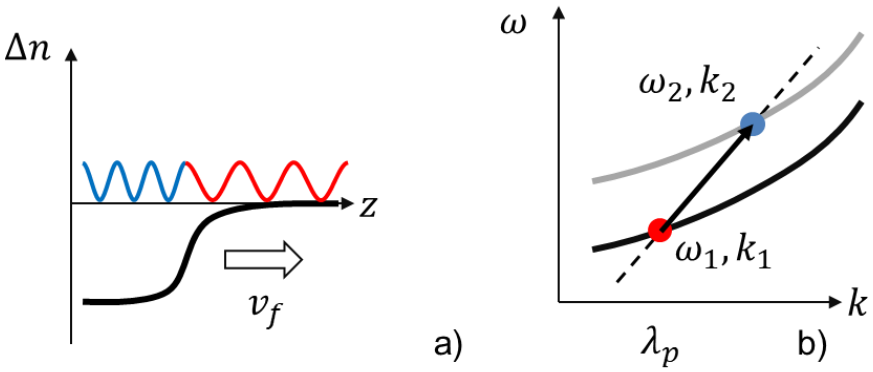

Figure 15: a) Schematic representation of a refractive index front in a waveguide. Negative change of refractive index is presented (black line), which shifts the dispersion of the waveguide upwards in frequency. The front is moving in the positive direction with velocity v_f. b) The schematic representation of the waveguide dispersion relation (band diagram in periodic systems) before the front arrived (black) and after the front passed by (grey). The monochromatic wave in the waveguide with original frequency ω_1 and wave number k_1 is transferred into the monochromatic wave with frequency ω_2 and wave number k_2. The line connecting these two points has a slope equal to front velocity $\Delta\omega/\Delta k = v_f$.

A special case is represented by a moving boundary between two media. We looked at a particular situation of a moving front inside an optical waveguide. To discuss reflection from such a front we first looked at the transmission case where the optical wave goes through the front. To switch the waveguide dispersion, we employed a switching optical pulse that generates free carriers in the silicon waveguide and reduces its refractive index (as shown in Figure 15 a). We consider a wave that goes through the boundary generated by the front. For this case we identified a condition of changing frequency and wavenumber of light. The same as in refractive optics the phase is conserved at the boundary between two media. In stationary optics that leads to Snell's law or conservation of the tangential component of the wavevector. At moving boundary, the phase continuity $\omega_1\Delta t - k_1\Delta x = \omega_2\Delta t - k_2\Delta x$ leads to the conservation of the ratio between change of frequency and change of wavenumber which is equal to the front velocity $\Delta\omega/\Delta k = \Delta x/\Delta t = v_f$. After this condition is known, similar to wavevector diagram the final state after the front can be identified. It is given by the intersection of the phase continuity line (dashed line in the Figure 15 b) with the dispersion relation of the perturbed waveguide (grey line). Due to change of both frequency and wave number, this was called an indirect transition.

It should be mentioned that reflection at a moving mirror, known as Doppler effect, also changes the frequency of light. But real objects are moving with velocities much smaller than speed of light, thus the frequency shifts are small. The fronts induced by other optical pulses, often called pump pulse, can generate fronts moving with a comparable velocity as that of the light signal in the medium or even faster, depending on the group velocity of pump pulse in the waveguide. At the same time these fronts are quite weak and lead to only small changes of the refractive index, which cannot be used to implement a mirror directly. Still for strong reflection dispersion of photonic crystal waveguides can be used as we show later.

[P13] E. A. Ulchenko, D. Jalas, A. Yu. Petrov, M. Castellanos Munoz, S. Lang, and M. Eich, "Pulse compression and broadening by reflection from a moving front of a photonic crystal," Opt. Express 22, 13280–13287 (2014).

My contribution was the idea to compress a pulse by a photonic crystal front, supervision of theoretical calculations and simulations, input to the publication.

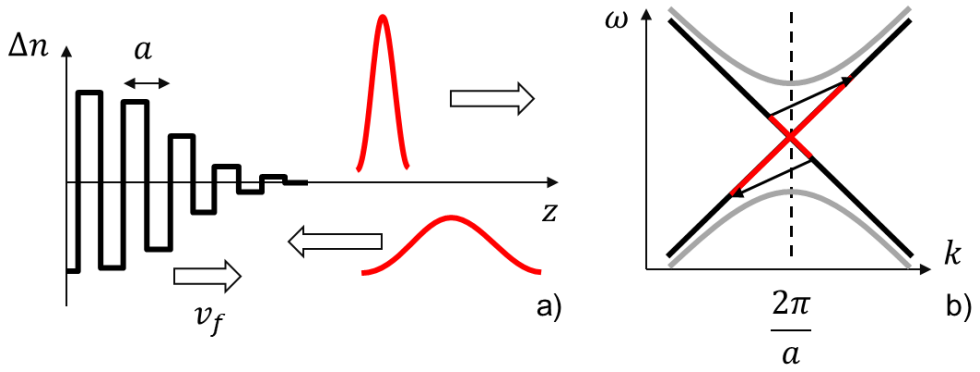

Figure 16: a) Schematic presentation of a photonic band gap front. The boundary between photonic crystal and homogenous medium is moving with front velocity v_f, the photonic crystal itself is not moving. The incident pulse at the frequency corresponding to the band gap of the photonic crystal is reflected with significant pulse compression. The signal velocity is larger than the front velocity. b) Schematic band diagram and the indirect transition during reflection from a photonic band gap front. In the homogeneous medium the dispersion relation shows no band gap (black lines), in the case of the refractive index perturbation the dispersion shows a band gap opening, with dispersion for the largest perturbation shown (grey line). Phase continuity lines are parallel to the arrows shown in the graph. Initially, light is positioned on the dispersion curve of unperturbed system with negative slope, moving in negative direction. The phase continuity lines do not intersect the maximally perturbed dispersion relation, thus no transmission of the signal into photonic crystal is possible. Light is projected on the dispersion curve with positive slope and thus is reflected back into homogeneous medium. During reflection a strong increase of frequency and wavenumber range is observed, that leads to pulse compression in time and space.

The first structure that we proposed for the reflection from the moving front was the moving boundary of a photonic crystal. In this case the periodic perturbation of refractive index gradually changes between periodic and homogeneous media and the boundary moves with the velocity comparable to the speed of

light. To understand the reflection, we again involve the projection of the states in the dispersion diagram using phase continuity lines. At the same time, the dispersion relation is not just shifted as in a previous publication [P12] but is changing from dispersion without band gap to dispersion with band gap. If the front would not move the signal would reflect if its frequency bandwidth would fall inside the band gap of the photonic crystal. In this case the frequency and duration of the signal would not change. If we increase the front velocity, the phase continuity lines start to intersect with the dispersion relation for reflected wave with a frequency offset. Thus, the initial frequency range is projected on a large frequency band without changing the center frequency of light. This results in the temporal compression of the reflected signal without change of its center frequency. The compression factors can be large depending on the front velocity. It increases when the front velocity is approaching the velocity of the reflected wave. It should be mentioned that a similar compression would be observed in the Doppler effect when light is reflected from a moving mirror. But to achieve order of magnitude compression factors mirror would have to move with velocity close to speed of light and there will be also order of magnitude shift of the central frequency.

Thus, moving photonic crystal fronts realize Doppler-like effects without actually moving material in space. The proposed effect was not demonstrated so far. It can be realized e.g., by lifting a degeneracy between two coupled periodic waveguides with a free carriers generated by a pump pulse. The group velocity of the pump pulse would define then the front velocity.

[P14] M. A. Gaafar, D. Jalas, L. O'Faolain, J. Li, T. F. Krauss, A. Yu. Petrov, and M. Eich, "Reflection from a free carrier front via an intraband indirect photonic transition," Nat. Commun. 9, 1447 (2018).

My contribution was the idea to reflect light in the forward configuration, supervision of theoretical calculations, simulations and characterization, input to the publication.

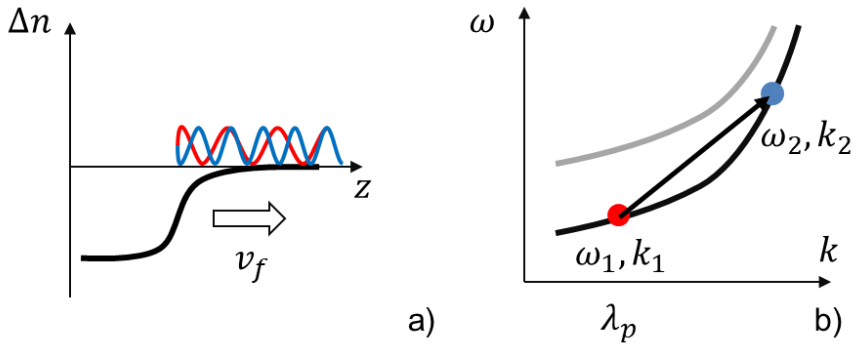

Figure 17: a) Schematic presentation of light reflection from a free carrier front. The initial wave propagating in the positive direction (red wave) is reflected in the forward direction and changes its wavelength (blue wave). b) The schematic dispersion relation and front induced transition. The front velocity is larger than the initial signal velocity (slope at red dot) and smaller than the final signal velocity (slope at blue dot). The phase continuity line does not cut through dispersion relation after the front (grey line) and light cannot transmit through the front.

Simpler as the realization of the moving photonic crystal boundary is the shift of the dispersion relation. We have recognized that if the pump pulse group velocity is correctly chosen, then signal light cannot

transmit through the front and is pushed to reflect in the forward direction with a new frequency (Figure 17 a). In this case the pump pulse can be chosen with the frequency between initial and final frequency of the signal, but also in a different frequency range where group velocity can be matched.

This forward reflection also leads to time reversal of the signal. Thus, the trailing edge of the initial signal pulse becomes the leading edge of the final signal pulse. Apart of reflection multiple other effects were predicted and demonstrated based on front induced transitions with the main contribution of the Dr. Mahmoud Gaafar:

M. A. Gaafar, A. Yu. Petrov, and M. Eich, "Free Carrier Front Induced Indirect Photonic Transitions: A New Paradigm for Frequency Manipulation on Chip," ACS Photonics 4, (2017).

M. A. Gaafar, T. Baba, M. Eich, and A. Yu. Petrov, "Front-induced transitions," Nat. Photonics 13, 737 (2019).

M. A. Gaafar, H. Renner, A. Yu. Petrov, and M. Eich, "Linear Schrödinger equation with temporal evolution for front induced transitions," Opt. Express 27, 21273 (2019).

M. A. Gaafar, J. Holtorf, M. Eich, and A. Yu. Petrov, "Pulse time reversal and stopping by a refractive index front," APL Photonics 5, 080801 (2020).

M. A. Gaafar, H. Renner, M. Eich, and A. Yu. Petrov, "Fourier optics with linearly tapered waveguides: Light trapping and focusing," APL Photonics 6, 066108 (2021).

5. Conclusion and outlook

We have shown several approaches to theoretically model light reflection from structured media. Generally, the vectorial wave equation should be solved to obtain results in all their complexity. But for special cases useful approximations can be derived that can allow predicting reflection and, which is more important, allow optimization of existing structures and design of new structures. We have developed further and applied these approximations to tailor the reflection from plasmonic metamaterials, photonic crystals, disordered media and moving fronts.

In this thesis mostly the optical properties of structured media were discussed without consideration of the manufacturing. The discussed structures were produced with our cooperation partners by different means like 1D thin film technology [P8, P9], 2D lithography [P1, P12, P14] and 2D and 3D self-assembly [P2, P3, P5, P7] and self-organization [P10, P11]. The self-assembly still stays the major route to obtain 3D structures with feature size comparable or smaller than wavelength of visible and NIR radiation [8], [9]. But truly optimized structures might require exact reproduction of the designed geometry which is not possible by conventional self-assembly. The improvement of 3D printing with voxels smaller than 100 nm might allow direct printing of designed structures for the NIR where the writing speed will be a major parameter [10], [11]. Alternatively, self-assembly with prescribed pair interactions can be envisaged with methods such as DNA origami [12], [13].

Another important development of structured materials is the possibility to change their properties under applied stimulus [14], [15] or even adaption of their properties to reduce the impact of the stimulus [16]. Such tunable or switchable optical materials are required for optical elements, such as lenses or spatial light modulators [15]. This functionality is also considered for large scale optical applications, such as smart surfaces or windows, which interact with visible and near IR sun radiation differently depending on temperature or weather conditions [17], [18]. Tunable thermal emission can be used for cooling at ambient temperatures [19].

We have optimized the structures based on human intuition. Another very promising direction is the structure optimization via automated inverse design. The solution of the vectorial wave equations can be used to identify reflection from a structured medium. Such problems can be efficiently addressed by analytical and numerical models. But the inverse problem where the spectral and directional reflection is defined and a corresponding structure for such functionality should be found is a complex nonlinear problem. Recently, with the development of computing facilities and numerical methods iterative approaches are successfully applied to converge to optimal designs [20]. Here, the obtained structures often do not follow the human design intuition and utilize the full complexity of free form geometry.

On the other hand, even the increase in computational power is sometimes not sufficient to provide high throughput electromagnetic simulations, especially in 3D geometries. Here, the development of machine learning tools based on artificial neural networks are consider to be useful to, first, predict the optical output of the structured medium, and, second, even solve the inverse problem by fast iterations of forward solutions or by direct understanding of structure – property relations [21]–[23]. Nevertheless, the handy analytical models and human intuition based on a wide spectrum of different problems still is a driving force behind the innovation so far. But in future deep neural networks might also enter this realm of human activity looking for new geometries and novel optical effects. Such neural networks can check solutions based on physical principals, interpret data and discover underlying physical mechanisms [23].

6. References

[1] A. Poddubny, I. Iorsh, P. Belov, and Y. Kivshar, "Hyperbolic metamaterials," Nat. Photonics 7, 958 (2013).

[2] K. Mnasri, A. Khrabustovskyi, M. Plum, and C. Rockstuhl, "Retrieving effective material parameters of metamaterials characterized by nonlocal constitutive relations," Phys. Rev. B 99, 035442 (2019).

[3] J. D. Joannopoulos, S. G. Johnson, J. N. Winn, and R. D. Meade, *Photonic crystals: Molding the flow of light*. Princeton University Press, 2011.

[4] H. C. van de Hulst, *Light Scattering by Small Particles (Dover Books on Physics)*, 2nd ed. Dover Publications, 1981.

[5] W. Liu and Y. S. Kivshar, "Generalized Kerker Effects in Nanophotonics and Meta-Optics," Opt. Express 26, 13085 (2018).

[6] C. J. R. Sheppard, S. S. Kou, and J. Lin, "The Green-function transform and wave propagation," Front. Phys. 2, 012614 (2014).

[7] H. Kogelnik, "Coupled Wave Theory for Thick Hologram Gratings," Bell Syst. Tech. J. 48, 2909 (1969).

[8] Y. A. Vlasov, X. Z. Bo, J. C. Sturm, and D. J. Norris, "On-chip natural assembly of silicon photonic bandgap crystals," Nature 414, 289 (2001).

[9] S. H. Kim, S. Y. Lee, S. M. Yang, and G. R. Yi, "Self-assembled colloidal structures for photonics," NPG Asia Mater. 3, 25 (2011).

[10] V. Hahn *et al.*, "Rapid Assembly of Small Materials Building Blocks (Voxels) into Large Functional 3D Metamaterials," Adv. Funct. Mater. 30, (2020).

[11] M. Kadic, G. W. Milton, M. van Hecke, and M. Wegener, "3D metamaterials," Nat. Rev. Phys. 1, 198 (2019).

[12] S. Dey *et al.*, "DNA origami," Nat. Rev. Methods Prim. 1, 1 (2021).

[13] A. Kuzyk, R. Jungmann, G. P. Acuna, and N. Liu, "DNA Origami Route for Nanophotonics," ACS Photonics 5, 1151 (2018).

[14] F. Neubrech, X. Duan, and N. Liu, "Dynamic plasmonic color generation enabled by functional materials," Sci. Adv. 6, eabc2709 (2020).

[15] T. Badloe, J. Lee, J. Seong, and J. Rho, "Tunable Metasurfaces: The Path to Fully Active Nanophotonics," Adv. Photonics Res. 2, 2000205 (2021).

[16] A. Walther, "Viewpoint: From Responsive to Adaptive and Interactive Materials and Materials Systems: A Roadmap," Adv. Mater. 32, 1 (2020).

[17] M. Casini, "Active dynamic windows for buildings: A review," Renew. Energy 119, 923 (2018).

[18] Y. Ke *et al.*, "Smart Windows: Electro-, Thermo-, Mechano-, Photochromics, and Beyond," Adv. Energy Mater. 9, 1902066 (2019).

[19] Z. Li, Q. Chen, Y. Song, B. Zhu, and J. Zhu, "Fundamentals, Materials, and Applications for Daytime Radiative Cooling," Adv. Mater. Technol. 5, 1901007 (2020).

[20] S. Molesky, Z. Lin, A. Y. Piggott, W. Jin, J. Vucković, and A. W. Rodriguez, "Inverse design in

nanophotonics," Nat. Photonics 12, 659 (2018).

[21] S. So and J. Rho, "Designing nanophotonic structures using conditional deep convolutional generative adversarial networks," Nanophotonics 8, 1255 (2019).

[22] W. Ma, Z. Liu, Z. A. Kudyshev, A. Boltasseva, W. Cai, and Y. Liu, "Deep learning for the design of photonic structures," Nat. Photonics 1 (2020).

[23] P. R. Wiecha, A. Arbouet, C. Girard, and O. L. Muskens, "Deep learning in nano-photonics: inverse design and beyond," Photonics Res. 9, B182 (2021).